# MODELLING OF THE DRIVING PROCESS OF L-SHAPED METAL SHEETS

Z. Yang, B. Lohmann

Technische Universität München, Munich

Corresponding author: Z. Yang, Technische Universität München, Inst. f. Automatic Control
85748 Garching, Boltzmannstraße 10, Munich,

**Abstract.** *Driving* is an incremental forming method. It has been used for centuries, but been researched very little in scientific fields. The driving is carried out by means of so called "Kraftformer" machines using universal tool sets. It can create almost any 2D or 3D geometries of metal sheets. But there exist very high interactions between the metal sheet and the tool in the driving process, where the vertical force from the tool is transformed in the horizontal directions and the metal sheet is clamped by the tool then to be stretched or shrinked. In the modelling, the geometry of the L-shaped metal sheets is approximated in the two combined flanks with constraints on the common edge. The employed material models are elastic-ideal plastic and elastic-real hardening. The force transformation is clarified in the tool model. Furthermore, there are three phases in the model of the forming: mixed elastic and plastic deformations; pure plastic deformation; springback and inverse bending. In the evaluation, the simulation and experiment results match to each other very well, so that the total model is suitable for model based applications.

## 1   Introduction

The Driving process nowadays is based on an incremental method for sheet metal forming with significantly reduced investment expenses. This technique which has not yet had much relevance in scientific considerations is one of the oldest metal forming processes available and has been used for centuries.

The driving process today solely requires a small low cost press (so called "kraftformer" machines) (see Fig. 1) and is able to shape metal sheets in 2D or 3D geometry using universal tool sets [6]. Due to the very high proportion of manual work in the production process, driving is only employed nowadays for the manufacture of niche products, e.g. for repairing and maintenance purposes in the aerospace industry, for panelling parts of railway cars, or for the restoration of vintage car bodies, i.e. for single parts and small quantities, where cost effectiveness is a minor issue, or where other forming processes fail.



**Figure 1:** Driving machine, so called "kraftformer" (left); Stretching and the structure of its used tools (right).

The Driving has a highly interactive process, in which material properties are changed by work hardening and where contact conditions are varied with every stroke. After a multitude of strokes, the shapes of the metal sheets suffer from accumulated inaccuracies. But in controlling or automating this forming process, an analytical model should be given to yield the corresponding parameters. Furthermore, such a model brings more knowledge of the internal forming procedures of the metal sheets, while FE model has not the ability to calculate the parameters due to its natural limitations and to be used in real-time control system. Hence, the driving process will be analytically modelled in this paper, although the high process interactions are mentioned in the above.

# 2   Modelling

Using the driving machine, the L-shaped metal sheets can be stretched or shrinked in processes by means of hammering strokes on the metal sheets. During every forming stroke, the tools clamp the sheet and transform the vertical stroke into horizontal movement and by that induce compressive (shrinking) or tensile (stretching) stress into the sheet. So the sheet can be bended at different positions into a given 2D form. The forming force can be applied manually or automatically by tuning the stroke depth, which denotes the distance between the upper and the lower tool part. In the paper, only the stretching process will be modeled.

## 2.1   L-shaped Metal Sheets

### 2.1.1   Approximated Geo-Model

The L-shaped metal sheets were finished by an edge bending machine before the beginning of the driving process. Such a sheet has two flanks and a transition zone between the both (see Fig. 2). In the forming process, the material of the upper flank is extended in the plain at the stroke position but in different rates. The nearer the stroke points are located at the transition zone, the less the material is elongated. The lower flank is orthogonal to the upper flank and is therefore only bended through the forming force of the upper flank. In order to make the analytical modelling of the stretching process easy, a Geo-Model is used to approximate the real sheet as the transitions zone is ignored and is replaced with the boundary conditions. There shows a shared fiber $_G\mathbf{f}$ jointing the two flanks. It is assumed that the transition zone of a L-shaped metal sheet can be hold very small during the edge bending.

### 2.1.2   Strains

In stretching process, the material of the $\pi_B$-flank is only extended, while the $\pi_H$-flank is compressed and tensioned around the common fiber respectively. Due to the boundary condition on the shared fiber, it yields a common bending angle $\theta$ (see Fig. 2). Actually, the length of the fiber $l_0$ changes only very small, so that the fiber is regarded as constantly long during the total process. The material of the fibers parallel to $_G\mathbf{f}$ in both flanks is elongated more or less alongside the fiber direction. Then the strains are formulated as defined in *small strain* in the following:

$$\varepsilon_{1B} = \int_{l_0}^{l_B} \frac{dl}{l} = \ln\left(\frac{l_B}{l_0}\right). \tag{1}$$

With the fiber length $l_B = \theta \cdot (\rho + y_B)$ at the position $y = y_B$ and

$$l_s = \theta \cdot \rho \tag{2}$$

, the strain $\varepsilon_{1B}$ is gained at the position $y_B$:

$$\varepsilon_{1B} = \ln(1 + \frac{y_B}{\rho}). \tag{3}$$

Due to the incremental forming, only a small strain can be gained at every increment, so that the strain can be linearized

$$\varepsilon_{1B} = \frac{y_B}{\rho}. \tag{4}$$

Similarily, the strain $\varepsilon_{1H}$ in the $\pi_H$-flank is $y_H/\rho$. Certainly, the strains can be calculated in *large strain* that is suitable for the large deformations [2]. But for this incremental stretching process, the sheet is formed in a small deformation at a forming step and can also achieve a certain large deformation after many forming steps.
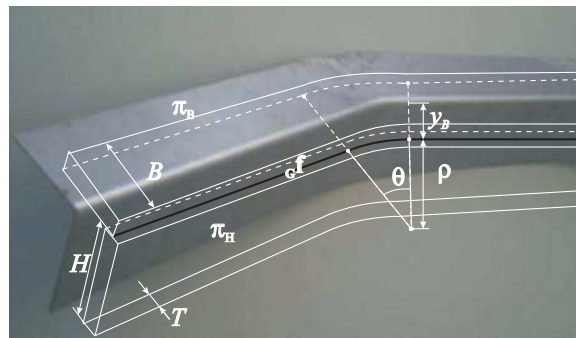


**Figure 2:** L-shaped metal sheet and its approximated Geo-model.
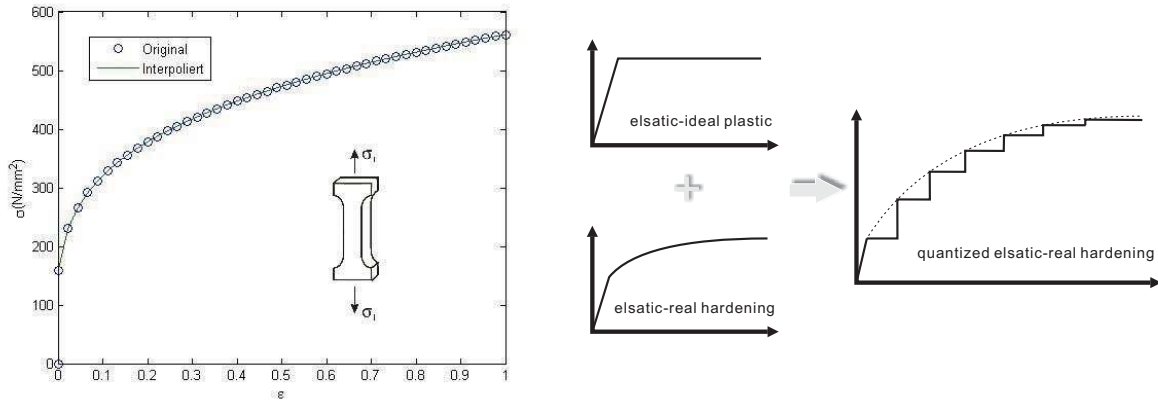
**Figure 3:** Flow curve on flat drawing (left); Quantized elastic-ideal plastic material model (right).

### 2.1.3 Material Models

In the stretching process, the deformations can be measured with the known sensors [5]. The first principal strain $\varepsilon_1$ is then calculated with the linearized strains. But the stresses can be only determined with the help of the material model in the forming procedures that characterizes the behaviour of the material under external forces in elastic and also plastic deformations. To gain the $\sigma_1 - \varepsilon_1$ relation firstly in the elastic domain, the stress-strain states

$$\pi_B : \begin{matrix} \varepsilon_1; & \varepsilon_2; & \varepsilon_3; \\ \sigma_1; & \sigma_2 = 0; & \sigma_3 = 0. \end{matrix} \qquad \pi_H : \begin{matrix} \varepsilon_1; & \varepsilon_2 = 0; & \varepsilon_3; \\ \sigma_1; & \sigma_2; & \sigma_3 = 0. \end{matrix} \tag{5}$$

are given according to the external foreces. With respect to the hook's law, the modulus of elasticity is $E/(1-v^2)$ for the $\pi_H$-flank ($v$ is the poisson's number) and $E$ for the $\pi_B$-flank. The stress $\sigma_1$ increases in proportion to the strain $\varepsilon_1$, but only till the elastic limit. Hereby, the limit is defined at the 0.2% plastic strain because of no distinct yield points on the stress-strain diagram. If the stress is beyond this limit, the flanks lie in plastic deformations. To describe it, the flow curve is used, from which not only the local state values such as stresses and strains but also the process values e.g. forces, energies, powers can be evaluated. The flow curve is plotted through the standardized plane drawing. It shows strain-hardening deformations in the reality. Alltogether, the elastic-real hardening model will be used for calculating the state values in the total stretching process. Furthermore, due to the incremental forming procedures, the elastic-ideal plastic model will be adopted during every forming increment to make the calculations simple. That is to say, the used elastic-real hardening model is quantized through the forming increments (see Fig. 3(right)).

### 2.2 Tools

The tool has two parts that press the sheet together so as to transform the vertical force in the horizontal direction. Each part has two movable sections that can be pushed horizontally to the sides by the transition elements of the tool parts.

#### 2.2.1 Stroke Movement

The needed forces to form the metal sheets are brought through the released strokes. The continuous movement $H_{st}$ of the upper tool is characterized by a sinusoidal function:

$$H_{st} = H_r + A_{st} \cdot \sin \omega t, \tag{6}$$

where $H_r$ is the reference position that can be adjusted by the operating panel or via a external control program, $A_{st}$ is the amplitude of the movement around the reference position and $\omega$ is the circle frequence of the movement. During the continuous movement of the upper tool, the strokes hitting the metal sheets can be released by an eccentric tappet. The rate of a stroke is defined as the stroke depth $h$ that indicates the further movement from the lowest point of the continuous movement deep into the metal sheets. A stroke movement is still sinusoidal but with a different amplitude:

$$H_{st} = H_r + (A_{st} + h) \cdot \sin \omega t. \tag{7}$$

The stroke depth can be tuned in the same way as the reference position. It should be denoted that the stroke movement happens only in the half period of the continous movement.

### 2.2.2 Load Transmission

The vertical forces $F_v$ corresponding to a reference position and a stroke depth can be measured through a load cell. The force response rises and falls with the moving of the tool (see Fig. 4 (left)). The maxima of the forces referring to an identical reference position and however different stroke depths appear in a linear relation to the stroke depth (see Fig.4 (center)).
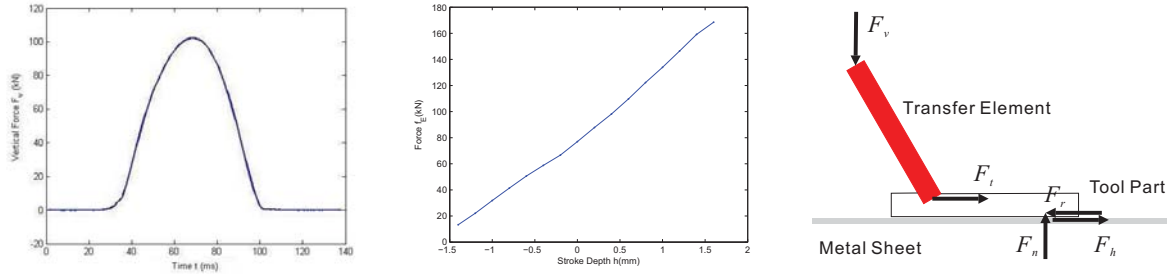


**Figure 4:** Vertical force response (left); Force progression on stroke depthes (center); Force transfering (right).

Because the final position at a stroke movement is equal to $H_r + A_{st} + h$, the identical maxima of the forces can be obtained at the different reference position but with the congruent stroke depth, althrough the force progressions could be different along the time axis. The maxima of the forces will be used to reconstruct the force progression for the load transmission into the metal sheet. The vertical force $F_v$ can be transfered via the transfer elements into the horizontal direction while the half tools move itself to the sides (see Fig. 4 (right)). The balance of the forces gives the following relations:

$$F_v = F_n; F_t = F_n / \tan(\alpha), \tag{8}$$

in which $\alpha$ is the angle of the transfer element according to the horizontal direction. The transfer force $F_t$ increases with decreasing the angle $\alpha$ when the normal force $F_n$ stays unchanged. However, the horizontal force $F_h$ on the metal sheet depends on the relative movement between the tools and the sheet. Hereby, the friction factor plays the role and will be explained in the next section.

### 2.2.3 Friction Factor

Actually, the force transfers in the horizontal direction are completed through the frictions between the tools and the sheet. Thereto, it is necessary to distinguish the frictions on sliding and adhering. With respect to the coulomb's law, the frictional force can be given as follows:

$$F_r = \mu_r \cdot F_n; \ F_h = F_r, \tag{9}$$

in which $\mu_r$ is the friction coefficient. But when the transfer force $F_t$ is less than $F_r$, the tools adhere on the sheet and move with it together. As the transfer force $F_t = F_n / tan\alpha$ is known, the friction coefficient $\mu_r$ and the transfer coefficient $\mu_t = 1/tan(\alpha)$ have the following relations:

$$\begin{cases} \frac{\mu_r}{\mu_t} < 1 \ on \ sliding \\[2mm] \frac{\mu_r}{\mu_t} \geq 1 \ on \ adhering \end{cases} \tag{10}$$

At this point, the friction factor $\mu = \mu(\mu_r, \mu_t, t_r)$ can be defined to describe the frictions during the transfer moving. However, it is not possible to know when the sliding finishes and the adhering begins, how the angle $\alpha$ changes. In oder to determine the friction factor, the FEM-simulation is used too identify the transfer coefficient, friction coefficient and the time range. From the results of the FEM-simulations [4], the friction coefficient was found out in the range $[0.36, 0.38]$. The tools slide then through the sheet without no adhering, because $\mu_r/\mu_t \geq 1$ can not be reached in the permitted range $[pi/6, pi/3]$ of the angle $\alpha$. In the reality, the friction factor changes stochastically after every stroke and therefore includes a random function in the modelling. In addition, the metal sheets have a small friction coefficient at the beginning.

### 2.3 Forming Procedures

In stretching processes, the strokes are released consecutively at different stroke positions with different stroke depths. During one stroke, the upper tool moves itself to the upper surface of the sheet and the successive forming procedure begins. There are totally three forming phases at the stroke (see Fig. 5). In the first phase, the two flanks are formed till the flow limits, while the second phase describes the pure material flows. When the stresses lie

again under the flow limits during unloading, the two flanks spring back but in different rates, so that the inverse bending of one flank is driven by the other flank.
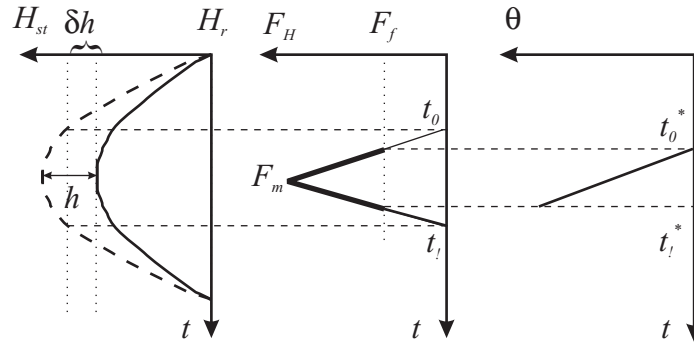


**Figure 5:** Progressions of the sinusoidal stroke movement, the horizontal force and the bending angle

### 2.3.1 Hybrid Deformations

In this phase, the two flanks are elastically formed at first. The bending moment of the $\pi_B$-flank is calculated as follows [1]:

$$m_{eB} = \int_0^B \sigma T dy \cdot y = \int_0^B T y^2/\rho \, dy = \frac{ETB^3}{3\rho}. \tag{11}$$

Certainly, the plastic deformations appear first of all on the boundaries, that is to say, the stress $\sigma_{1B}$ reaches the flow limit $S_B$ at $y = B$, which yields the elastic curvature limit and the elastic moment limit

$$\left(\frac{1}{\rho}\right)_{eB} = \frac{S}{BE}, \tag{12}$$

$$m_{lB} = \frac{B^2 T S_B}{3}. \tag{13}$$

Furthermore, the hybrid (or elastic-plastic) deformations happen in the flanks with the distributions of the stresses (see Fig. 6).
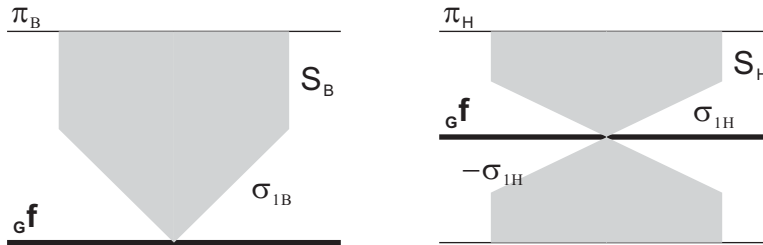


**Figure 6:** Distributions of the stresses of the two flanks.

The ratio between the elastic and the plastic deformation is defined with the curvature $r_B = (1/\rho)_{eB}/(1/\rho)$ and therefore the bending moment is newly formulated in the following:

$$m_{epB} = \int_0^{y_e} \sigma_{1B} T dy \cdot y + \int_{y_e}^B S_B T dy \cdot y = \frac{1}{6} S_B T B^2 (3 - r_B^2), \tag{14}$$

where $y_e = \rho S_B/E = B \cdot r_B$.

Altogether, the moments for the $\pi_H$-flank can be calculated in the similar way and finally it yields the following moment vectors:

$$\mathbf{m}_e = \begin{pmatrix} m_{eB} \\ \frac{\overline{E}HT^3}{12\rho} \end{pmatrix}, \mathbf{m}_{ep} = \begin{pmatrix} m_{epB} \\ \frac{1}{12} S T^2 H(3 - m_H^2) \end{pmatrix}, \mathbf{m}_l = \begin{pmatrix} m_{lB} \\ \frac{BT^2 S_H}{6} \end{pmatrix} \tag{15}$$

The external moment $m_w = l_h \cdot F_h$ ($l_h = \int y dA / \int dA$)) balances the combined moments of the two flanks during different deformation states:

- Step 1: $m_w = \mathbf{i}^T \cdot \mathbf{m}_e$ – both flanks in pure elastic deformations;

- Step 2: $m_w = \mathbf{i}_e^T \cdot \mathbf{m}_e + \mathbf{i}_p^T \cdot \mathbf{m}_{ep} - \pi_B$-flank in hybrid deformation and $\pi_H$-flank still in elastic deformation;
- Step 3: $m_w = \mathbf{i}^T \cdot \mathbf{m}_{ep}$ – both flanks in hybrid deformations,

in which $\mathbf{i} = (1\,1)^T$, $\mathbf{i}_e = (0\,1)^T$, $\mathbf{i}_p = (1\,0)^T$.

After step 2, the bending angle

$$\theta = \frac{2S_H l_0}{\overline{E}T} \tag{16}$$

is reached. At the end of the step 3, if the horizontal force beyonds the force limit

$$F_f = \frac{1}{4}(2B^2 S_B + HTS_H)/l_h, \tag{17}$$

the two flanks are going to the pure material flows, which will be clarified in the next section.

### 2.3.2 Material Flows
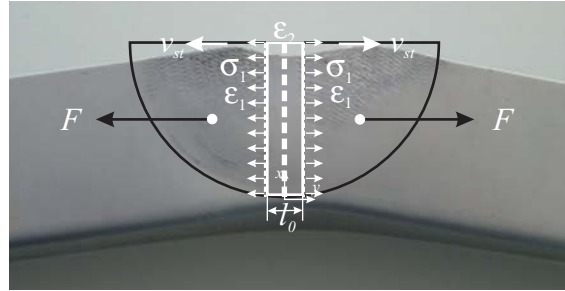


**Figure 7:** Strain-stress state on the sheet during the material flow.

Actually, the bending angle is determined by the boundary elongation of the $\pi_B$-flank, so that the deformation at $y_B = B$ can be seen as uniaxial. The $\pi_H$-flank is formed passively and its deformation can be ignored in this phase because of its small forming widerstand. To describe the forming states, the deformation state variale $\mathbf{e} = (\varepsilon_{1B}\ \dot{\varepsilon}_{1B})^T$ is defined and it has the following dynamics:

$$\dot{\mathbf{e}} = \begin{pmatrix} 0 & 1 \\ 0 & 0 \end{pmatrix} \mathbf{e}; \tag{18}$$

$$\theta = (\frac{l_0}{B}\ 0) \cdot \mathbf{e}|_{y=B}, \tag{19}$$

in which the state variable $\mathbf{e}$ is dependent on a position and there is the boundary condition $\mathbf{e}|_{y=0} = 0$. The deformation velocity $\dot{\varepsilon}_{1B}$ is determined by the displacement velocity $v_{1B}$ [3] or

$$\dot{\varepsilon}_{1B} = \partial v_{1B}/\partial x. \tag{20}$$

The velocity $v_{1B}$ depends on the horizontal velocity $V_{st}$ of the tool parts:

$$v_{1B} = \frac{2V_{st}}{Bl_0}xy. \tag{21}$$

The velocity $V_{st}$ can be approximately resulted from the function of the stroke movement (see Eqn. **??**), or

$$V_{st} = \frac{1}{2}\frac{\partial H_{st}}{\partial t}\Big|_{t=t_0^*}, \tag{22}$$

in which the material begins to flow at the time $t_0^*$. It is assumed that the velocity stays constant in the total flow time interval. Thus, the state varialble $\mathbf{e}$ at the boundary $y = B$ is given as follows:

$$\mathbf{e}|_{y=B} = (\frac{2V_{st}}{l_0}\Delta t\ \ \frac{2V_{st}}{l_0})^T. \tag{23}$$

The progression of the stroke movement indicates that the upper tool contacts the upper surface of the sheet since the time point $t_0$ (see Fig. 5). At the time point $t_0$, the slackness between the sheet and the tool is removed and the lower tool does not slacken any more. Since this time point

$$t_0 = \frac{1}{\omega}\arcsin\left(\frac{A_{st} + \delta h}{A_{st} + h}\right), \tag{24}$$

the force on the sheet rises linearly to the maximum $F_m$ and then falls off. Hereby, $\delta h$ indicates the slackness between the upper tool and the sheet and the slacked offset of the lower tool. It is formulated as follows:

$$\Delta h = \xi \frac{\overline{H} + \overline{h}}{H_r + h} h, \tag{25}$$

where $\xi$ is the transfer factor that describe the effect of the initial movements of the tools in vertical and horizontal directions, in which the slackness disappers and the tools don't slide on the surfaces any more. The reference distance $\overline{H} + \overline{h}$ is brought in the calculation because the tool moves itself from a reference position. The value $\overline{H}$ and $\overline{h}$ can be arbitrarily chosen in the valid intervals with suitable $\xi$. Since the time point

$$t_1 = \frac{1}{\omega} \left[ \pi - \arcsin \left( \frac{A_{st} + \delta h}{A_{st} + h} \right) \right], \tag{26}$$

the upper tool leaves from the surface. In the time interval $[t_0^*, t_1^*]$, the material flows when the horizontal force $F_h$ exceeds the limit $F_f$ (Eq. **??**). Hereby, the leverage $l_h$ is equal to the width of the $\pi_B$-flank under the assume of the uniaxial deformation. The flow time vector is calculated as follows:

$$\mathbf{t}^* = \begin{pmatrix} t_0^* \\ t_1^* \end{pmatrix} = \begin{pmatrix} 1-\eta & \eta \\ \eta & 1-\eta \end{pmatrix} \cdot \mathbf{t}, \tag{27}$$

where $\eta = \frac{F_f}{2\mu F_m}$ and $\mathbf{t} = (t_0\ t_1)^T$. It should be denoted that the necking and thinning are not regarded.

### 2.3.3 Springback and Reverse Bending

If the force $F_h$ falls below $F_f$, the bended L-sheet springs back. To calculate the springback angle $\theta_z$, the similarity law of triangles is used on the flow curve and

$$\theta_z = \frac{S_B L}{E B}. \tag{28}$$

Actually, the flank $\pi_H$ has also a springback angle that ist different from $\theta_z$, so that the flank $\pi_H$ should be bended back to find a new forming balance. Because the springback angles are even very small, the reverse bending is ignored here.

## 3   Evaluation

To evaluate the model, the L-shaped metal sheets are standardized with the following parameters

$$B = 35mm, H = 50mm, T = 1mm, l_0 = 9mm, E = 210kN/mm^2, \nu = 0.3.$$

The system and model parameters are

$$H_r = 23.5mm, A_{st} = 3.9mm, \omega = 2\pi/0.138kHz, h \in [0.5mm, 2.0mm], \xi = 0.78$$

that describe the stroke movements. The friction factor $\mu$ is formulated with a random function

$$\mu = \begin{cases} 0.05 & at\ the\ first\ stroke \\ 0.36 + 0.2 \cdot Rand() & since\ the\ second\ stroke \end{cases} \tag{29}$$

to simulate the stochastic changing of the surface roughness one after another stroke.
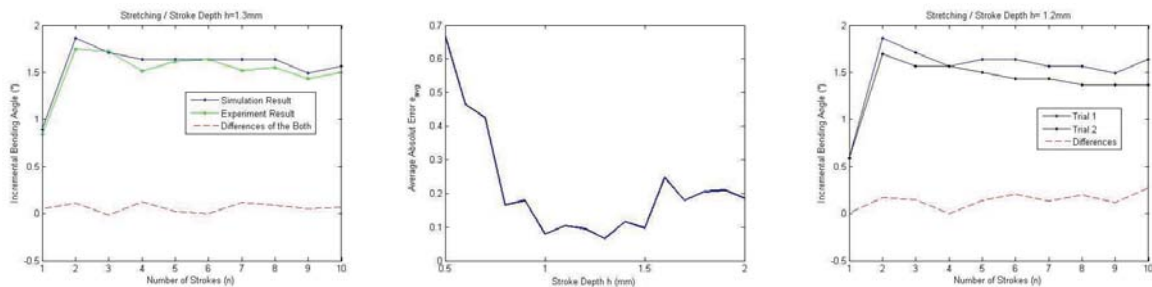


**Figure 8:** Simulation and Experiment result on the stroke depth $h = 1.2mm$ (left); The average absolute errors on stroke depths (center); Two identical trials but given the different results (right).

The experiments are carried out using the standardized stahl sheets, for each of which ten strokes are released with an identical stroke depth. The Fig. 8 shows the incremental bending angle on the simulation and the experiment with the stroke depth $h = 1.2mm$. Firstly, the strain-hardening procedure can be identified. Because of the stochastic changing of the surface roughness, exact matching between the both can not be reached. Hereby, the average absolute error

$$e_{avg} = \frac{1}{N}\Sigma_{i=1}^{N}|\theta_i^{sim} - \theta_i^{exp}| \tag{30}$$

is employed to valuate the modelling. As seen in the Fig. 8, the most errors lie under 0.2 with the stroke depth $h$ from 0.8$mm$ to 2.0$mm$. Actually, it gives different results even on two identical trials (see Fig. 8). The model can not give good results any more on the stroke depths $h = 0.7mm, 0.6mm$ and 0.5$mm$. On the one hand, the force response along the time axis becomes more highly nonlinear because of the strongly reducing of the vertical forces, so that the flow time interval $[t_0^* \, t_1^*]$ can not be estimated very well. On the other hand, the forming of the $\pi_H$-flank has more effects that on the other stroke depths.

## 4    Summary and Outlook

The stretching (or driving) process has high interactions between tools and materialien. To model this process, the Geo-model was established to approximate the real geometry of the sheets. From the Geo-model, the strains in the two flanks were formulated and linearized. The stresses were calculated with respect to the quantized elastic-real hardening model. The tools bring the forces into the sheets during its sinusoidal stroke movements. The vertical load is transfered in the horizontal direction by the transfering elements. The friction factor effects the horizontal force of the sheet very highly, so that the sheet experiences hybrid deformations, material flows and springback. The simulation and experiment results can not match each other exactly. But the average absolute error $e_{avg}$ can be acceptable on the most stroke depths according to the stochastic changing of the surface roughness.

In the future, a complexer Geo-model can be used, so that the deformation of the sinuous transition zone will be not ignored. The strain must not be linearized and the real material model will be used also during each forming increment. If the response of the vertical force and the deformation of the sheet can be simultaneously measured, the assume of the uniaxial material flow in the $\pi_H$-flank must be involved to make the model also on the small stroke depths more precisely. Altogether, this model can be as basic principles for the modelling of the shrinking processes and can be used in the real-time control applications.

## 5    References

[1] Marciniak Z., Duncan J. L. and Hu S. J.: *Mechanics of Sheet Metal Forming*. Butterworth-Heinemann, 2002.

[2] Wagoner R. H. and Chenot J. L.: *Fundamentals of Metal Forming*. John Wiley & Sons, Inc., 1997.

[3] Doege E. and Behrens B. A.: *Handbuch Umformtechnik*. Springer-Verlag, Berlin, 2007.

[4] Hoffmann H. and Petry R.: *Mass Customization of Sheet Metal Parts by Numerically Controlled Driving*. In: SheMet05 - International Conference on Sheet Metal, Erlangen, 2005.

[5] Yang Z., Markert M., Scherer D., Golle M., Weber S., Hoffmann H., Lohmann B. and Lüth T. C., *A Human-Machine interactive Driving System*. In: IEEE International Conference on Distributed Human-Machine Systems, Athens, Greece, March 2008.

[6] N. N: *www.eckold.com*.